

# The Role of the Initiator System in the Synthesis of Acidic Multifunctional Nanoparticles Designed for Molecular Imprinting of Proteins

Marwa Aly Ahmed<sup>1,2</sup>, Júlia Erdőssy<sup>1</sup>, Viola Horváth<sup>1,3\*</sup>

<sup>1</sup> Department of Inorganic and Analytical Chemistry, Faculty of Chemical Technology and Biotechnology, Budapest University of Technology and Economics, H-1111 Budapest, Szent Gellért tér 4., Hungary

<sup>2</sup> Department of Chemistry, Faculty of Science, Arish University, 45511 El-Arish, North Sinai, Dahyet El Salam, Egypt

<sup>3</sup> MTA-BME Computation Driven Chemistry Research Group, H-1111 Budapest, Szent Gellért tér 4., Hungary

\* Corresponding author, e-mail: [vhorvath@mail.bme.hu](mailto:vhorvath@mail.bme.hu)

Received: 11 December 2019, Accepted: 03 April 2020, Published online: 24 August 2020

## Abstract

Multifunctional nanoparticles have been shown earlier to bind certain proteins with high affinity and the binding affinity could be enhanced by molecular imprinting of the target protein. In this work different initiator systems were used and compared during the synthesis of poly(*N*-isopropylacrylamide-co-acrylic acid-co-*N*-tert-butylacrylamide) nanoparticles with respect to their future applicability in molecular imprinting of lysozyme. The decomposition of ammonium persulfate initiator was initiated either thermally at 60 °C or by using redox activators, namely tetramethylethylenediamine or sodium bisulfite at low temperatures. Morphology differences in the resulting nanoparticles have been revealed using scanning electron microscopy and dynamic light scattering. During polymerization the conversion of each monomer was followed in time. Striking differences were demonstrated in the incorporation rate of acrylic acid between the tetramethylethylenediamine catalyzed initiation and the other systems. This led to a completely different nanoparticle microstructure the consequence of which was the distinctly lower lysozyme binding affinity. On the contrary, the use of sodium bisulfite activation resulted in similar nanoparticle structural homogeneity and protein binding affinity as the thermal initiation.

## Keywords

poly(*N*-isopropylacrylamide) nanoparticle, tetramethylethylenediamine, sodium bisulfite, initiator, protein binding

## 1 Introduction

Since the seminal paper of Pelton and Chibante [1], thermoresponsive poly(*N*-isopropylacrylamide) nanoparticles (NPs) have attracted a rapidly growing interest which does not seem to level off even in the last ten years. This is due to their unique reversible Volume Phase Transition (VPT) upon thermal stimuli at near-physiological temperatures. In addition, by copolymerizing other functional monomers with *N*-isopropylacrylamide (NIPAm), NPs with novel properties can be obtained with extended applicability. These novel "smart" materials that respond to pH, ionic strength, solvent and other environmental changes besides thermal stimuli can be used in numerous fields [2] like drug-delivery [3, 4] biosensing [4, 5] catalysis [6] and optical devices [7]. An intriguing application area of such nanoparticles is stemming from Shea's group who applied them as plastic antibodies that are capable of recognizing

specific biomacromolecules with effectiveness comparable to antibodies [8]. Water soluble NPs having high affinity to a toxic target peptide, melittin were synthesized by free-radical copolymerization of NIPAm with hydrophobic and charged monomers in the presence of a small amount of crosslinker (*N,N*-methylenebisacrylamide, BIS) based on the methods of Debord and Lyon [9] and Ogawa et al. [10]. By optimizing the type and ratio of the monomers to match hydrophobic and charged amino acid sequences in the peptide high affinity multifunctional copolymer nanoparticles could be obtained [11]. Furthermore, by applying affinity purification [12] or combinatorial approach [13] the affinity of the NPs to the target peptide could be largely enhanced. The NPs with enhanced binding affinity showed neutralization of the toxin in vivo [14]. A similar strategy was involved by the same group to design high affinity

multifunctional NPs for the selective capture and thermocontrolled release of a protein, lysozyme, whereby the thermoresponsivity of the polyNIPAm particles was also exploited [15]. These particles autonomously switching to the collapsed state above their VPT temperature, encapsulated the protein preventing it from denaturation upon thermal stress [16]. Later, along the same line NPs have been developed with nanomolar affinity for other proteins, too [17, 18]. In order to further increase the affinity of these biomolecule-selective NPs molecular imprinting appears to be a promising strategy [19–21]. Molecular imprinting creates molecular recognition sites in a polymeric material by copolymerizing monomers and crosslinker in the presence of the target or template molecule, which is removed from the ensuing 3D polymer network. Imprinted binding sites being complementary in shape and functional groups to the template can then selectively rebind it with high affinity. Such an approach has been used by Shea's group to obtain high affinity NPs for the peptide melittin [22]. Other groups have adapted the multifunctional nanoparticle approach to prepare protein imprinted NPs using solid phase anchored templates [23–27]. In these polymerization systems the original, persulfate initiated precipitation polymerization method [9, 10] which was carried out in the presence of a surfactant at 60 °C, had to be modified because these circumstances are not favorable for the imprinting of the delicate proteins. The high temperature required for the fast decomposition of ammonium persulfate (APS) initiator could be alleviated by applying an activator. Tetramethylethylenediamine (TEMED) is widely used with APS as a redox pair to initiate the polymerization of acrylamide hydrogels under mild circumstances and has been introduced for the preparation of poly(NIPAm) nanogels as well by Hu et al. [28]. The above cited, protein imprinted multifunctional NPs have been also synthesized using the APS/TEMED redox pair. Another, less frequently used reducing agent with APS is sodium bisulfite (SBS) [29]. Our aim was to study how the different initiator systems influence the properties of multifunctional poly(NIPAm) nanoparticles in order to achieve favorable protein binding affinities under optimal polymerization conditions for molecular imprinting. Until now, there have been very few research conducted to reveal the differences in the micro/hydrogel properties obtained with different initiator systems [30–33]. In this paper, therefore, we have compared the physico-chemical properties, the polymerization rate and lysozyme binding properties of poly(*N*-isopropylacrylamide-co-*N*-*tert*-butylacrylamide-co-acrylic

acid) nanoparticles proposed by Yoshimatsu and utilized by others [15, 17, 24, 26, 34–36] using different initiation systems. We have used ammonium persulfate at 60 °C both in surfactant-free precipitation polymerization and also using SDS and the redox systems APS/TEMED and APS/SBS at room temperature and at 40 °C.

## 2 Material and methods

### 2.1 Chemicals

*N*-isopropylacrylamide (NIPAm), acrylic acid (AAc), *N,N*-methylene bisacrylamide (BIS), ammonium persulfate (APS), sodium dodecyl sulfate (SDS), *N,N,N',N'*-tetramethylethylenediamine (TEMED), sodium bisulfite (NaHSO<sub>3</sub>; SBS), freeze-dried *Micrococcus lysodeikticus*, lysozyme from chicken egg white (MW 14.3 kDa, pI 11.35) were from Sigma-Aldrich. *N-tert*-butylacrylamide (TBAm) was purchased from Tokyo Chemical Industry Co. All chemicals were used as received, except that NIPAm was recrystallized from hexane and AAc was passed through an aluminium oxide inhibitor remover column (Sigma-Aldrich) before use. Ultrapure water was produced by a Millipore Direct-Q system (Merck). Gradient grade acetonitrile and hexane were from Merck. Ortho-phosphoric acid 85 % was from VWR International.

### 2.2 Preparation of the polymer nanoparticles

The feed monomer composition of the NPs, the initiators and other additives used during their synthesis are listed in Table 1. NIPAm, AAc, BIS and in one instance SDS (10 mg) were dissolved in water (50 mL) and the resulting solution was filtered through a 0.2 µm regenerated cellulose membrane filter to remove particulate impurities. TBAm was dissolved in ethanol (1 mL) before addition to the monomer solution. The total monomer concentration was 65 mM. Argon gas was bubbled through the reaction mixture for 50 minutes. Following the addition of 300 µL freshly prepared 100 mg/mL aqueous APS solution (4 mol% of the polymerizable double bonds) and 19.4 µL TEMED or 135 µL 100 mg/mL SBS the polymerization was carried out in a thermostated water bath for 3 h under continuous magnetic stirring and argon bubbling. The polymerization solution was purified by dialysis (Spectra/Por 4 type RC membrane, 12–14 kDa MWCO, Spectrum Laboratories Inc., Rancho Dominguez, CA, USA) in ultrapure water changed twice a day for 5 to 6 days to remove unreacted monomers and impurities. The yield of the NPs was determined by measuring their weight after drying at 60 °C for one day. The dilution due to dialysis was taken into correction.

**Table 1** Polymerization conditions used during the synthesis of the nanoparticles

Sample name	Monomer composition [mol%]				Initiator system (molar ratio of the components)	Temperature [°C]
	AAC	TBAc	NIPAm	BIS		
NP1*	5	40	53	2	APS	60 °C
NP2	5	40	53	2	APS	60 °C
NP3	5	40	53	2	APS:SBS (1:1)	40 °C
NP4	5	40	53	2	APS:SBS (1:1)	RT
NP5	5	40	53	2	APS:TEMED (1:1)	40 °C
NP6	5	40	53	2	APS:TEMED (1:1)	RT
NP7	2.5	40	55.5	2	APS:TEMED (1:1)	40 °C
NP8	10	40	48	2	APS:TEMED (1:1)	40 °C
NP9	5	40	53	2	APS:TEMED (1:0.5)	40 °C
NP10	5	40	53	2	APS:TEMED (1:0.25)	40 °C

\* polymerization was carried out in the presence of 0.2 mg/mL SDS

### 2.3 Measurement of the hydrodynamic diameter and the zeta potential

The zeta potential and the hydrodynamic diameter of the NPs were measured with a Zetasizer Nano-ZS instrument (Malvern Instruments, Malvern, UK). The dialyzed NP solution was transferred into a disposable cuvette and the hydrodynamic diameter was measured in three replicates at  $25 \pm 0.1$  °C by Dynamic Light Scattering (DLS). Polydispersity index (PDI) was calculated by the instrument as the width of a hypothetical monomodal distribution. Before zeta potential measurements the dialyzed nanoparticles were diluted ten times with water and placed into a zeta potential cell that had been thoroughly cleaned with ultrapure water. Each reported zeta potential is the average of three successive measurements.

### 2.4 Determination of the Volume Phase Transition Temperature (VPTT) of the NPs

The VPTT of the NPs in water was studied by dynamic light scattering measurements at different temperatures. Before each measurement the solutions were incubated at the specified temperature for 25 min to achieve thermal equilibrium. Each point represents an average of 3 replicate measurements.

### 2.5 Measurement of monomer conversion

To follow the monomer conversion, samples were taken regularly from the polymerization reaction mixture at different time intervals. The samples were immediately diluted with ultrapure water and oxygen was introduced to stop the reaction. Unreacted monomers were separated from the polymeric reaction products by filtration

through an 0.2  $\mu\text{m}$  regenerated cellulose membrane filter and the filtrate was analyzed by high-performance liquid chromatography (HPLC) measurements. The monomers were quantified using an EX1600 HPLC system (Exformma Technologies, China) equipped with UV detector. The stationary phase was a Lichrospher 100 C18 column (125 mm  $\times$  4 mm i.d., 5  $\mu\text{m}$ ) from Merck KGaA. A mixture of 95 % water, 5 % acetonitrile and 0.05 % ortho-phosphoric acid was used as the mobile phase with a flow rate of 2.0 mL min<sup>-1</sup>. The injection volume was 25  $\mu\text{L}$ . The detector wavelength was set to 210 nm.

### 2.6 Scanning electron microscopic analysis of the NPs

Before the measurement the NP sample was diluted with water and ultrasonicated for 30 mins. One drop of polymer suspension was placed onto a copper grid with continuous carbon layer and dried at room temperature. The microstructure of the nanoparticles was studied using a Hitachi S-4800 Field Emission Scanning Electron Microscope (SEM) equipped with Bruker AXS Energy-dispersive X-ray spectrometer (EDS) system. An acceleration voltage of 10 kV was used for the analysis and secondary electron (or transmitted electron) signals were used to study the morphology of the polymers. Particle size was determined from the SEM micrographs by averaging the diameter of at least 100 individual particles from each sample using the ImageJ 1.52a software (National Institutes of Health, Bethesda, MD, USA). Polydispersity index (U) was calculated using the following formulas.

$$D_n = \frac{\sum_{i=1}^K n_i D_i}{\sum_{i=1}^K n_i} \quad (1)$$

$$D_w = \frac{\sum_{i=1}^K n_i D_i^4}{\sum_{i=1}^K n_i D_i^3} \quad (2)$$

$$U = D_w / D_n \quad (3)$$

where  $D_n$  is the number-average diameter,  $D_w$  is the weight-average diameter and  $U$  is the polydispersity index.  $D_i$  denotes the individual diameter of a particle,  $n_i$  is the number of particles with a specific diameter, and  $k$  is the number of different diameters.

### 2.7 Lysozyme binding to the NPs

Lysozyme (5  $\mu\text{g/mL}$ ) was incubated with various concentrations of the NPs (between 0.5 and 2000  $\mu\text{g/mL}$ ) in phosphate buffer (PB, 10 mM, pH 7.4) for 20 minutes at room temperature. A Vivaspin 500 (100 kDa MWCO) centrifugal filter unit (Sartorius Stedim Lab Ltd., Stonehouse, UK) was utilized to separate the free and NP-bound lysozyme by centrifugation (Eppendorf 5430R, Eppendorf AG, Hamburg, Germany) at 11,800 rcf for 20 minutes. The lysozyme activity of the filtrate was measured and compared to that of a similarly filtered 5  $\mu\text{g/mL}$  control lysozyme solution ( $B_0$ ). The ratio of the two gives an estimate of unbound/total lysozyme concentration. Subtracting this ratio from 1 gives the ratio of the protein bound to the NPs ( $B$ ) relative to the initial protein concentration ( $B_0$ ).

### 2.8 Lysozyme activity assay

Lysozyme activity assay was based on the method of Shugar [37]. 5  $\mu\text{g/mL}$  lysozyme was dissolved in PB (10 mM, pH 7.4). Freeze-dried *Micrococcus lysodeikticus* cells were resuspended at 150  $\mu\text{g/mL}$  concentration in PB (50 mM, pH 6.2). 100  $\mu\text{L}$  lysozyme containing solution was added to 2500  $\mu\text{L}$  cell suspension, and the cell lysis was followed at 25  $^\circ\text{C}$  by measuring the decrease in absorbance at 450 nm using a UV-Vis spectrophotometer (JASCO V-550, JASCO International Co. Ltd., Tokyo, Japan). The slope of absorbance decrease in the first 5 minutes was used as a measure of lysozyme activity.

## 3 Results and discussion

### 3.1 Preparation of the nanoparticles

We have prepared thermoresponsive polymer nanoparticles from NIPAm, AAc and TBAm monomers with 2 mol% BIS crosslinker using different initiator systems. Table 1 shows the feed monomer composition and other synthesis conditions of the nanoparticles. The molar ratio of the monomers in samples NP1-NP6 and NP9-NP10 was the same as described by Yoshimatsu et al. [15] who optimised

multifunctional NPs for the sequestration of lysozyme, an antimicrobial enzyme with high isoelectric point (11.35). 53 mol% NIPAm served as a backbone monomer, 40 mol% TBAm afforded hydrophobic character and 5 mol% AAc provided negative charge to the nanoparticle. It was shown earlier [15] that both the hydrophobic and negatively charged monomers are indispensable for the binding of the positively charged protein. Moreover, the incorporation of high percentage of TBAm into the poly(NIPAm) backbone lowered the VPTT from 32  $^\circ\text{C}$  to approximately 11  $^\circ\text{C}$ , therefore free-radical precipitation polymerization at room temperature became feasible. Polymers NP7 and NP8 contained half as much and two times more acrylic acid, respectively compared to the others. In two samples the polymerization was initiated with APS only (NP1; NP2) and the polymerization temperature was set to 60  $^\circ\text{C}$  since the decomposition rate of APS is insignificant at room temperature and still quite low at 40  $^\circ\text{C}$ . Sodium-dodecylsulfate surfactant was added to the monomer mixture of NP1 to obtain small particles below 100 nanometer [5] but it was omitted in case of NP2 (surfactant-free polymerization). To carry out the polymerization at (25  $^\circ\text{C}$ ) or near room temperature (40  $^\circ\text{C}$ ), besides APS, tetramethylethylenediamine (NP5-NP10) or sodium bisulfite (NP3; NP4) was added to increase the decomposition rate of APS. These latter circumstances are adaptable in the molecular imprinting of proteins since the lower temperatures and the omission of surfactant are favorable for these biomolecules.

All the polymerizations resulted in homogeneous, milky polymer suspensions even when cooled down to room temperature and in each case the yield was above 80 % (Table 2). At room temperature all the polymers were still in a collapsed state due to the incorporated hydrophobic TBAm monomer. The suspension of nanoparticles prepared with (NP1) and without SDS at 60  $^\circ\text{C}$  (NP2) and using SBS (NP3; NP4) was stable even after months. On the contrary, nanoparticles prepared with TEMED (NP5-NP10) settled down in less than an hour (Fig. 1).

### 3.2 Characterization of the nanoparticles

Morphology of the different nanoparticles was studied by scanning electron microscopy. SEM micrographs of NP1, NP2, NP3 and NP5 are shown in Fig. 2 a)–d).

NP1, NP2 and NP3 consisted of both single beads and small aggregates of 2 to 10 uniformly sized particles. From the SEM images it can be perceived that the aggregates are formed during the polymerization process whereby the particles grow together at some point.

**Table 2** Particle size, zeta potential and yield of the nanoparticles

Sample	Hydrodynamic diameter <sup>a</sup> [nm]	PdI <sup>b</sup>	Dry particle diameter <sup>c</sup> [nm]	U <sup>d</sup>	Zeta-potential [mV]	Yield [%]
NP1	85.9±1.7	0.031	70.2±9.4	1.057	-41.5	88.4
NP2	444.9±8.9	0.043	374±22	1.011	-42.6	83.1
NP3	168.0±3.4	0.060	152±14	1.026	-41.6	88.7
NP4	173.8±1.7	0.069	-	-	-40.0	86.4
NP5	213±12	0.241	93.4±6.7	1.015	-40.7	92.9
NP6	144±25	0.577	-	-	-32.7	86.4
NP7	139.0±7.0	0.096	-	-	-42.5	98.2
NP8	251.7±5.5	0.114	-	-	-35.7	89.3

<sup>a</sup> Number mean diameter measured by dynamic light scattering in water at 25 °C

<sup>b</sup> Polydispersity index obtained from DLS measurement

<sup>c</sup> Measured by SEM

<sup>d</sup> Polydispersity index obtained from SEM measurement

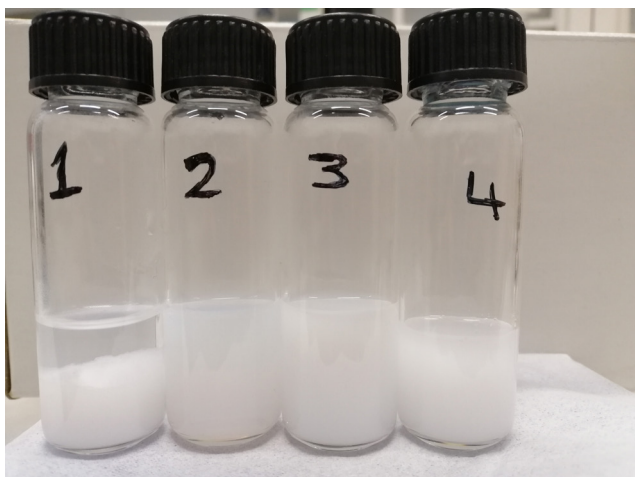


**Fig. 1** Snapshot of the nanoparticles after 1 hour settling (from left to right; 1 - NP5 prepared at 40 °C with TEMED; 2 - NP1 prepared at 60 °C using SDS, 3 - NP3 prepared at 40 °C using SBS; and 4 - NP2 prepared at 60 °C without SDS)

Contrary to NP1-3, NP5 prepared with TEMED contained much larger aggregates of hundreds of monodisperse particles. This can explain the fast settling time and the instability of its colloidal solution. The size of NP1, NP2, NP3 and NP5 in the dry state was determined from the SEM images. Particle sizes obtained with SEM together with the polydispersity indices ( $U$ ) are listed in Table 2.

Polymerization at 60 °C with surfactant yielded the smallest particle size (NP1; 70.2±9.4 nm), while the lack of SDS at 60 °C lead to several hundred nanometer particle diameter (NP2; 374±22 nm). The combined use of APS initiator and SBS yielded 152±14 nm particles (NP3) while APS with TEMED resulted in 93.4±6.7 nm particle size (NP5). It can be deduced that the use of the redox initiator systems, similarly to the use of a surfactant allowed the formation of much smaller particles than the

surfactant-free polymerization. All the particles showed very uniform size distribution with polydispersity indices being between 1.011 and 1.057. The size of the hydrated, collapsed nanoparticles was measured by dynamic light scattering in water at 25 °C (Table 2).

These values were approximately 10–20 % higher than the dry particle diameters in case of NP1-3, due to hydration and also to the presence of small aggregates that the DLS cannot resolve. Nonetheless, the particle size of NP5 measured by DLS was more than twice higher than the size obtained from SEM measurement. This is mainly attributable to the largely aggregated particles and not to extensive swelling. Size homogeneity obtained from the DLS measurements supported this assumption. Polydispersity indices (PdI) below 0.1 indicated that NPs prepared at 60 °C or with SBS (NP1-4) were highly monodisperse, while nanoparticles obtained using TEMED had a much broader size distribution (NP5-6). The Volume Phase Transition Temperature of NP1-6 was studied by measuring the hydrodynamic diameter of nanoparticles at different temperatures using DLS. Results of NP1-5 are shown in Fig. S1 a)–e) in the Supplement. (NP6 could not be measured due to its colloidal instability.) All polymer preparations exhibited similar VPT at around 10 °C in agreement with literature data for the same monomer composition [15]. Below the VPTT the NP solutions became completely transparent and no valid measurement results could be obtained, probably due to the very low scattering intensity. It can be concluded that the collapse temperature was not affected by the initiation method.

Zeta potential measurements in water were carried out to prove the incorporation of acrylic acid into the polymer NPs. For this purpose, a reference polymer containing 58 mol% NIPAm, 40 mol% TBAm and 2 mol% BIS but

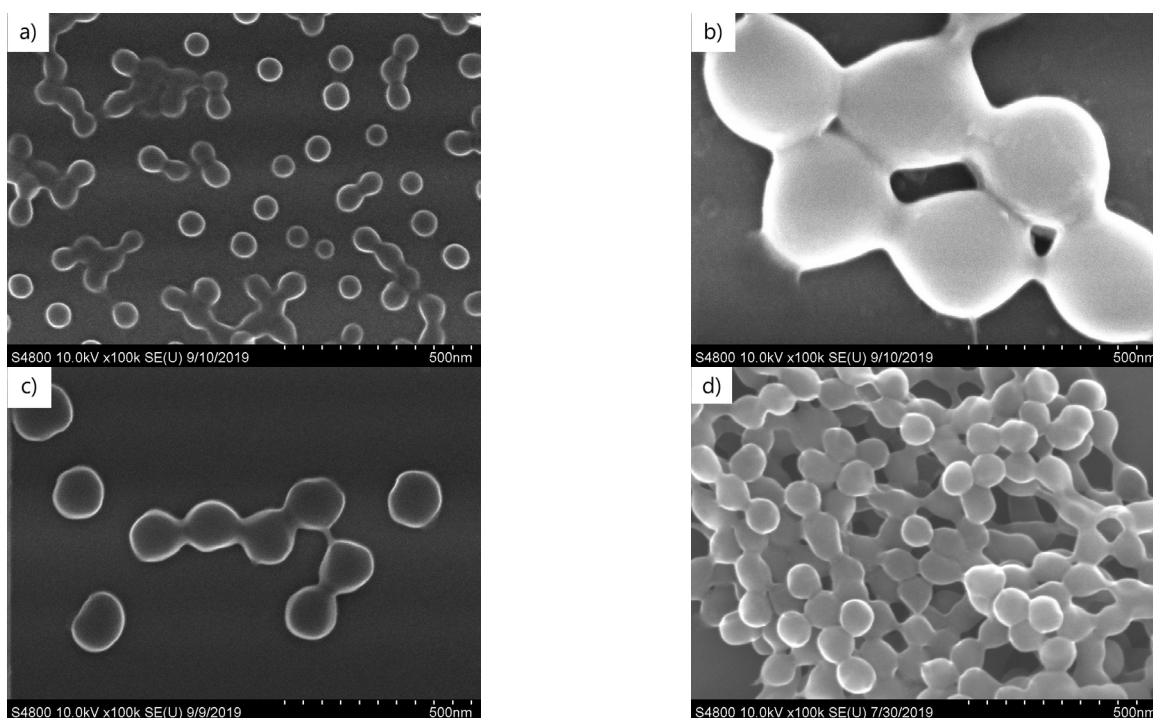


**Fig. 2** SEM images of NPs: a) NP1, prepared at 60 °C using SDS; b) NP2, prepared at 60 °C without SDS; c) NP3, prepared at 40 °C using SBS and d) NP5, prepared at 40 °C with TEMED. All pictures were taken at 100,000 times magnification

no acrylic acid has been synthesized at room temperature using the APS/TEMED initiator system. This polymer had a zeta potential of 7.47 mV. As can be seen in Table 2 all the NPs had much more negative zeta potential values than the reference polymer indicating that AAc was built into the polymer structure endowing the particle surface with negative charges. Interestingly, NP6 had less negative zeta potential (−32.7 mV) than NP5 (−40.7 mV), although they differed only in their polymerization temperature. Later experiments have shown that only 55 % of the feed AAc was incorporated into NP5 as opposed to 85 % in NP6 and this difference might have been the cause of the observed less negative surface charge.

### 3.3 Monomer conversion measurements

In order to investigate the polymerization kinetics and the extent to which the different monomers are incorporated into the polymer network we have followed the amount of residual monomers in time during the polymer synthesis. For this purpose, aliquots from the reaction mixture were taken at different time intervals and the residual monomers were quantitated by HPLC after filtration. Conversion of each monomer was calculated, together with the total monomer conversion. To compare the polymerization kinetics using the different initiator systems the total monomer conversion was plotted in time in Fig. 3. For the time course

of the individual monomer conversions see Fig. S2 in the Supplement. It can be noted at first glance that the polymerization rate using the redox initiator systems (NP3 and NP5) is much higher at 40 °C than with merely APS at 60 °C (NP1 and NP2). This is attributable to the much faster initiator decomposition rate in the redox system compared to its thermal homolysis [38, 39]. With SBS and TEMED maximum conversion is achieved already after about 40 minutes, while using only APS with and without SDS approximately 120 minutes is needed. It is also of interest to compare

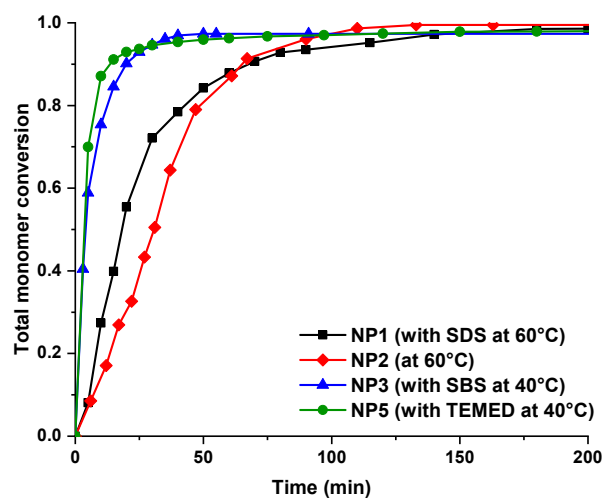


**Fig. 3** Total monomer conversion with time obtained with the different initiator systems

the polymerization rates of the two redox initiator systems at room temperature and at 40 °C (Fig. 4). With the SBS/APS system the rate of polymerization is much slower at room temperature (NP4) than at 40 °C (NP3), in fact it is similar to

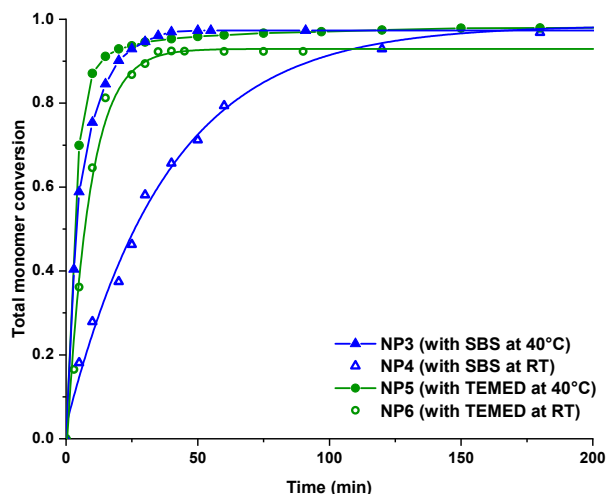


Fig. 4 Total monomer conversion using the redox initiator systems at different temperatures

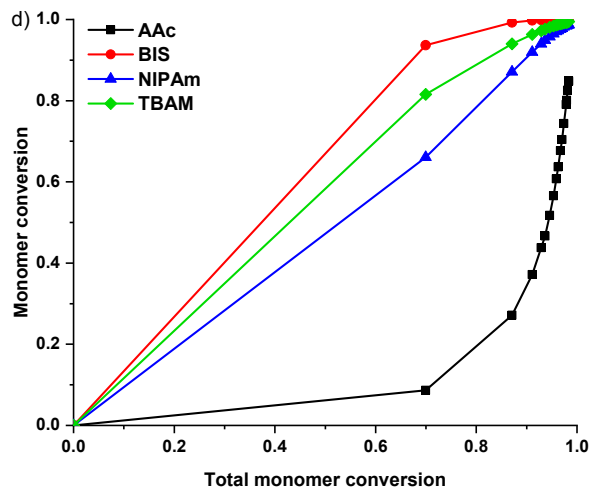
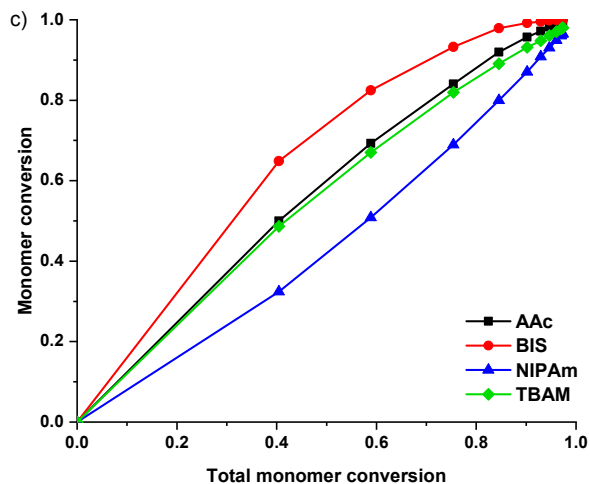
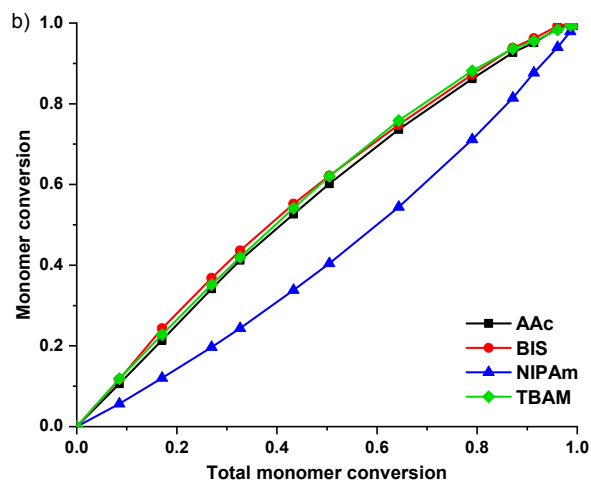
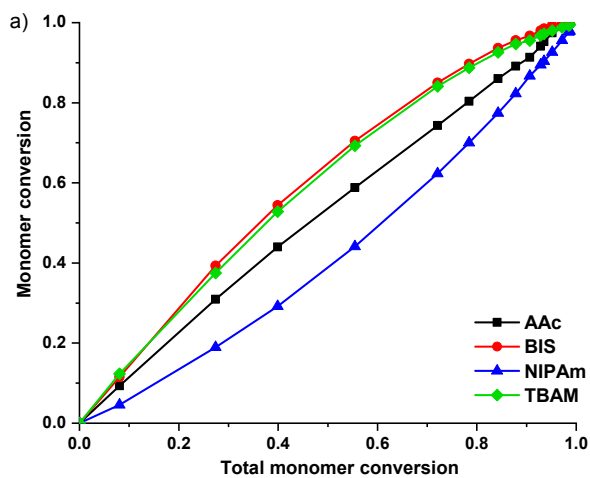


Fig. 5 Conversion of the different monomers as a function of the total monomer conversion a) NP1 prepared at 60 °C using SDS; b) NP2 prepared at 60 °C; c) NP3 prepared at 40 °C with the APS/SBS initiator system; d) NP5 prepared at 40 °C with the APS/TEMED initiator system

that of the polymerizations at 60 °C with only APS. On the contrary, using TEMED with APS the rate of polymerization is only slightly affected by the temperature.

To visualize the relative conversion rates of the individual monomers, their conversion was plotted against the total monomer conversion in the different polymerization systems (Fig. 5 a)–d)). In these plots if a monomer has a more positive curvature than the other it indicates that it is converted faster throughout the reaction. The relative incorporation rate of BIS, TBAM and NIPAm shows quite similar picture, only slight differences exist. In all systems the BIS crosslinker reacts faster than the other monomers and NIPAm is the slowest among the three.

This behavior has already been reported with NIPAm/BIS microgels [40] and has important consequences on the structural inhomogeneity of the microgel particle.

Because BIS incorporates faster into the growing microgel particles than NIPAm, the internal core of the particle has a higher crosslink density while the outer shell is composed of dangling branched polymer chains [41]. As far

as the AAc conversion is concerned, there is a striking difference between the TEMED/APS system and the others. Using APS with and without SDS at 60 °C and using the SBS/APS redox initiator system the relative incorporation rate of AAc is higher than that of NIPAm indicating that the core of the microgel particles is somewhat more enriched in AAc than the outer layers. This is in good agreement with the results of Hoare and McLean [42] who investigated the functional group distributions in carboxylic-acid-functionalized poly(NIPAm)-based microgels.

It is stunning to see, however, that using TEMED to catalyze the decomposition of APS, the polymerization rate of AAc drastically lags behind the others. Moreover, at the end of the reaction when all the other monomers are fully converted there is still significant amount (approx. 15 %) of unreacted AAc monomer in the polymerization mixture.

Hoshino et al. [12] have come to a qualitatively conforming conclusion when they measured the incorporated AAc to be 48 % at different AAc feed concentrations in a similar polymerization system. If we take a closer look on the polymerization rate of the individual monomers in the different polymerization systems (see Fig. S2 in the Supplement) it becomes evident that TEMED selectively enhances the polymerization rate of all the monomers, but acrylic acid. One can explain this by the acid base properties of the two substances: TEMED being a weak base ( $pK_a$  8.97) can react with acrylic acid, a weak acid ( $pK_a$  4.25) forming an acrylate salt. It was shown earlier for the free-radical polymerization of acrylic acid in aqueous solutions that by changing the pH from 1 to 7 and concomitantly neutralizing the acid the polymerization rate is rapidly decreasing [43–45]. This might be due to the inherently different polymerization rates of the protonated and deprotonated forms of acrylic acid. Therefore, by adding TEMED to the polymerization mixture where AAc is present in comparable quantity the acid will be neutralized (the degree of ionization is 0.8) and its polymerization slows down.

To clarify this behavior, first, we have changed the AAc feed concentration to half and double of the initial composition i.e. from 5 mol% (NP5) to 2.5 mol% (NP7) and 10 mol% (NP8) and carried out the polymerization using TEMED with APS at 40 °C.

In Fig. 6 a) the conversion of AAc during the three polymerization reactions is plotted with time. As demonstrated in the figure there is no significant difference in the rate of AAc conversion and the final monomer conversions are also equal in each case. The conversion of AAc is not complete, only 85 % of the initial amount is

polymerized. Concurrently, the AAc concentration in the final particles is somewhat less than 2.5; 5 and 10 mol%, that is 2.1; 4.3 and 8.8 mol%, respectively. However, if we plot the conversion of AAc against the total monomer conversion (Fig. 6 b)), one can observe important differences. With the lowest, 2.5 mol% AAc feed concentration the incorporation rate of AAc compared to the other monomers is the lowest and increasing the molar concentration of AAc its relative polymerization rate increases, the most explicitly with 10 mol% AAc. Since the polymerization rate of AAc is the same in all three systems, this must imply that the polymerization rate of the other monomers is decreasing by feeding more and more AAc (see Fig. S3 in the Supplement) This, in turn, suggests that excess AAc inactivates TEMED and its catalytic effect ceases. Caglio and Righetti have found that during polyacrylamide gel polymerization the APS/TEMED system

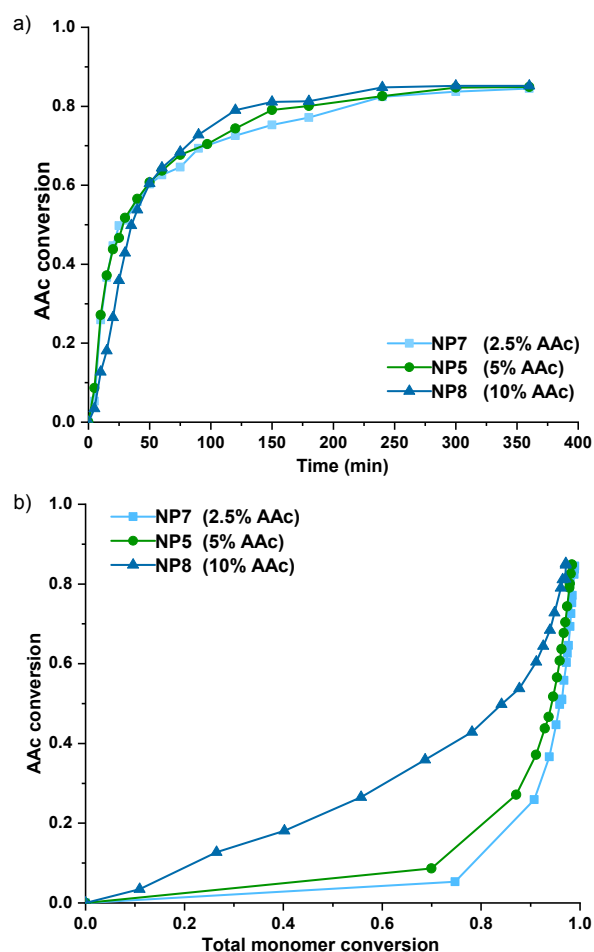


Fig. 6 a) Conversion of AAc as a function of time in NPs with different molar ratios of AAc in the presence of TEMED at 40 °C; b) Conversion of AAc plotted against the total monomer conversion in NPs with different molar ratios of AAc in the presence of TEMED at 40 °C

gives optimal incorporation of the monomers only in the 7–10 pH range and decreasing the pH the conversion drops markedly until at pH 4 no gelation occurs [46]. We have measured the pH in the monomer mixtures of NP7, NP5 and NP8, and it was found that increasing the molar concentration of AAc from 2.5 to 5 and 10 mol% the pH successively decreases from 8.3 to 6.0 and 5.0, respectively which eventuates that TEMED becomes less and less active, as we observed. It should be mentioned here, that the same authors suggested the concurrent use of SBS and TEMED to extend the optimal pH range of the acrylamide polymerization down to pH 4.

As a second step, we have decreased the amount of TEMED to 50 and 25 % of its original concentration in the polymerization solution, thereby changing the original APS/TEMED 1:1 molar ratio to 1:0.5 (NP9) and 1:0.25 (NP10) to see how this affects the polymerization rate. Polymerizations were carried out at 40 °C. The total monomer conversion with time and the AAc conversion against the total monomer conversion were plotted in these systems (Fig. 7 a) and b), respectively). (For the change of the individual monomer conversions with time see Fig. S4 in the Supplement).

From Fig. 7 a) one can see that by lowering the TEMED concentration from 100 % to 50 % and then to 25 % of its original value the polymerization becomes slower as can be expected in a common redox initiation system. Similar observation has been made by Feng et al. [47] in the solution polymerization of acrylamide. It can also be perceived that using 1:0.25 APS/TEMED molar ratio the polymerization practically stops well before the monomers are completely converted. The total monomer conversion is only 0.77. Fig. 7 b) indicates that by lowering the TEMED concentration the relative incorporation rate of AAc is getting higher approaching that of the polymers synthesized without TEMED. Here again, just like with increasing concentrations of AAc, this signifies that it is not the AAc who reacts faster, but the polymerization becomes slower and higher fraction of AAc remain in the neutral (protonated) form. (see Fig. S4 in the Supplement). Using 1:1 and 1:0.5 APS/TEMED ratio the final monomer conversion of AAc does not change ( $\approx 0.8$ ). In these samples the final monomer conversion of the other monomers approaches unity. With 1:0.25 APS/TEMED ratio the final conversion of AAc is less, only 0.67, but here the conversion of the other monomers is also incomplete.

The above results support the assumption that TEMED and AAc mutually affect each other during the polymerization. Excessive amounts of AAc shift the pH of the

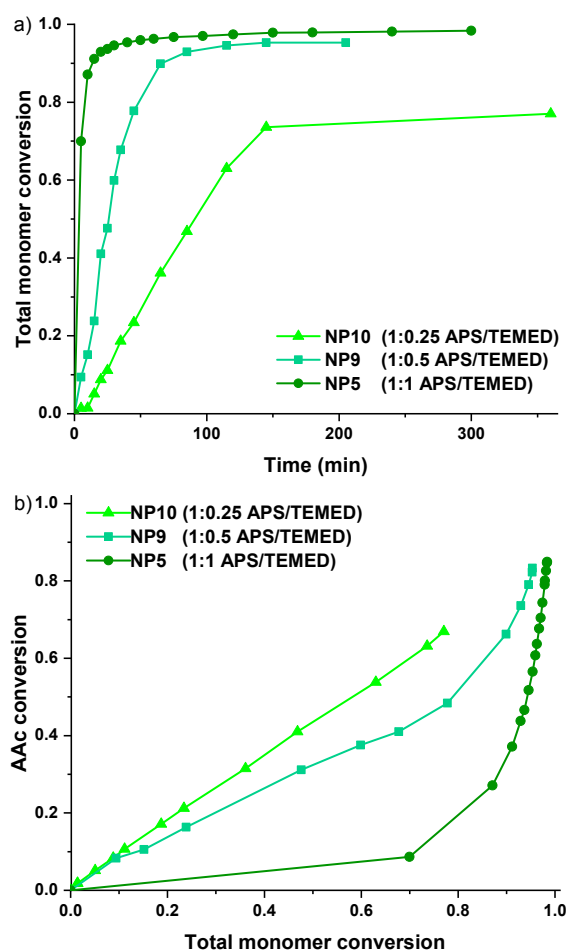


Fig. 7 a) Total monomer conversion with time in NPs prepared with different TEMED concentrations; b) Conversion of acrylic acid as a function of the total monomer conversion with varying TEMED concentrations

polymerization to lower pH values where the catalytic effect of TEMED is inhibited. On the other hand, while TEMED enhances the polymerization rate of NIPAM, BIS and TBA<sub>m</sub>, it slows down the polymerization of AAc by partially or completely neutralizing it and forming acrylate salt.

These effects result in two consequences considering the resulting microgel particles:

- Whereas not all of the AAc is converted during the NP synthesis the final monomer composition of the microgel particle is different from the feed monomer composition i.e. it contains less AAc. It is also different from the nanoparticles prepared with only APS at 60 °C with or without SDS or at 40 °C with SBS where all the monomers are fully converted.
- The microstructure of the particles synthesized using TEMED might be very different from that of the NPs prepared with the other initiation systems. While with the latter initiators AAc is converted somewhat

faster than NIPAm during microgel formation, using TEMED the opposite tendency prevails, that is AAC is converted much slower. Therefore, as opposed to the other polymers where the core of the particle is slightly enriched in AAC and the outer shell contains relatively lower concentrations, here the particle core has markedly lower AAC concentration while the outer surface is highly enriched in it. We have to bear in mind though, that the average AAC concentration in the particle is lower than in the other systems due to the incomplete conversion of AAC.

### 3.4 Lysozyme binding properties of the nanoparticles

In the next set of experiments, we have addressed, how the above differences in their microstructure influence the protein binding affinity of the nanoparticles. Thus we compared the lysozyme binding properties of NPs synthesized with the different initiator systems. Lysozyme binding to the NPs was assessed by incubating increasing concentrations of the nanoparticles with 5  $\mu\text{g/mL}$  protein then separating the bound and unbound protein by ultrafiltration. The lysozyme concentration in the filtrate (unbound concentration) was estimated with an enzymatic assay using *Micrococcus lysodeikticus* cell suspension as substrate. Ratio of the bound and total amount of lysozyme was plotted against the NP concentration. This plot can be seen in Fig. 8 a) for the differently initiated polymers.

At a first glance it is obvious that different concentrations are needed from the various nanoparticles (NP1; NP2; NP3 and NP5) to bind the same amount of lysozyme. This can arise from two aspects. First of all, due to differences in the size of the nanoparticles, their surface area available for protein binding is also different. Second, this can be also an indication that the NPs possess dissimilar affinities for the protein. In order to separate these two phenomena, we have calculated the bound amount of lysozyme per unit surface area which is independent of particle size. This has been estimated from the particle diameter and density and the initial, linear portion of the binding curve, where the particle surface is supposedly saturated with the protein using Eq. (4):

$$\frac{c_{Lys}}{\frac{c_{NP}}{\rho \times V_{NP}} \times A_{NP}} = \frac{c_{Lys}}{\frac{6 \times c_{NP}}{\rho \times d_H}}, \quad (4)$$

where:

- $c_{Lys}$  is the bound lysozyme concentration
- $c_{NP}$  is the weight concentration of the nanoparticles

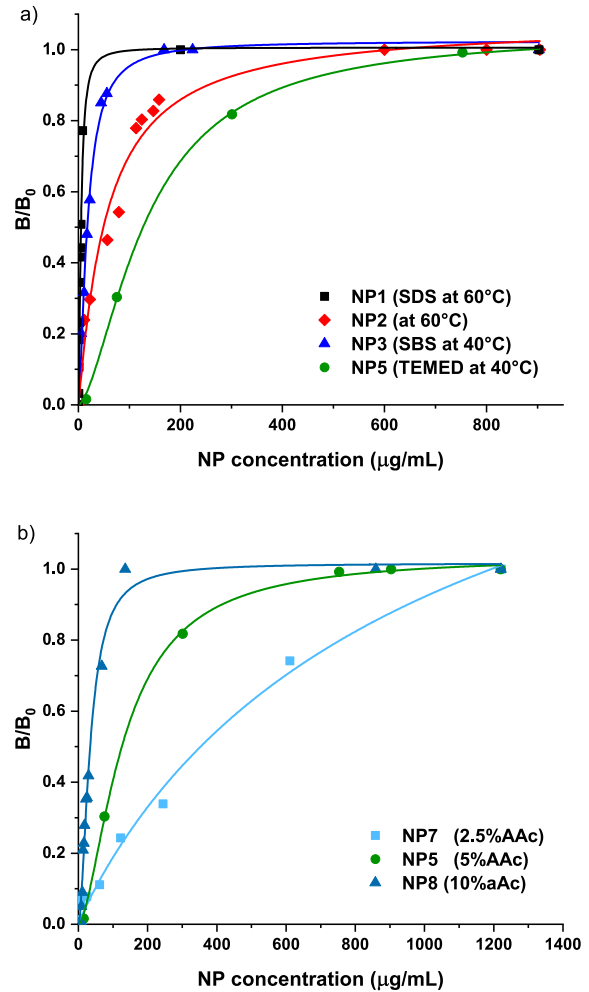


**Fig. 8** Bound/total lysozyme concentration with increasing nanoparticle concentration a) of NP1; NP2; NP3 and NP5 having the same feed monomer composition and b) of NP7; NP5 and NP8 having 2.5; 5 and 10 mol% AAC in the feed monomer mixture

- $\rho$  is the estimated density of the nanoparticle (0.27  $\text{g/cm}^3$ , taken from [11])
- $V_{NP}$  and  $A_{NP}$  is the volume and area of one nanoparticle, respectively
- $d_H$  is the hydrodynamic diameter of the nanoparticle

The results can be seen in Table 3 and they can be considered only as rough approximate values. As can be concluded from Table 3 NP1 (SDS at 60 °C), NP2 (at 60 °C) and NP3 (SBS at 40 °C) binds lysozyme in a similar order of magnitude. This suggests that they show similar affinity to the protein. Polymer NP5 (TEMED at 40 °C) binds almost an order of magnitude less protein showing a significantly decreased affinity. This can be interpreted using the results of the monomer conversion measurements. In NP1; NP2 and NP3 all the monomers are completely

**Table 3** Estimated lysozyme binding capacity of the nanoparticles

Sample	Hydrodynamic diameter [nm]	Bound lysozyme per unit surface area [ $\mu\text{g}/\text{m}^2$ ]
NP1	85.9 $\pm$ 1.7	1700
NP2	444.9 $\pm$ 8.9	1200
NP3	168.0 $\pm$ 3.4	1000
NP5	153.9 $\pm$ 5.5	250
NP7	139 $\pm$ 7.01	50
NP8	251.7 $\pm$ 5.5	700

converted and incorporated into the particles so the average particle composition is the same for all three samples.

The relative conversion rate of the monomers is also quite similar and, as a consequence the particle microstructure should be fairly homogeneous, the internal core of the particles is only slightly enriched in AAc compared to the outer surface.

On the contrary, in NP5 the AAc conversion is not complete, therefore its molar concentration in the final particle is less than in the three other NP samples. What is more important, its relative conversion rate is significantly lower than in NP1; NP2 and NP3, and the outer part of the nanoparticle contains almost all the incorporated AAc and much less from the other monomers. This implicates that the proper balance of the hydrophobic TBAM and the charged AAc monomer that is necessary to bind lysozyme [15] is not achieved and the NP has much lower affinity to the protein.

In a complementary set of experiments, we have compared the lysozyme binding affinity of NP7; NP5 and NP8 having 2.5; 5 and 10 mol% AAc feed concentrations, respectively. These results are shown in Fig. 8 b). As indicated in Fig. 8 b) increasing AAc content led to an increased lysozyme binding since less particle could bind the same amount of protein. To correct for the different surface areas of the NPs, the bound lysozyme per unit surface area has been calculated again and shown in Table 3. NP7 synthesized with the lowest AAc feed concentration showed the lowest binding affinity, the surface concentration of lysozyme being only 50  $\mu\text{g}/\text{m}^2$ .

Increasing the AAc feed ratio to 5 and 10 mol% resulted in correspondingly increased surface concentrations of 250 and 700  $\mu\text{g}/\text{m}^2$ , respectively. The increased concentration of the negatively charged monomer, however, cannot account for the large difference in the observed affinities in itself. The main reason is presumably the difference in the relative incorporation rates of AAc in NP5, NP7 and NP8 (see Fig. 6 b) and Fig. S3 in the Supplement)

and the evolving inhomogeneous monomer distributions across the nanoparticles. In NP7 with 2.5 mol% AAc feed concentration the particle surface is probably much more enriched in AAc than in NP8 with 10 mol% AAc, where the polymerization of the other monomers is much slower, therefore AAc is more homogeneously distributed in the particle. The more balanced hydrophobic and charged patches on the particle surface consequently ensure considerably higher binding affinity towards lysozyme.

#### 4 Conclusions

Different initiator systems have been compared for the synthesis of poly (*N*-isopropylacrylamide-co-acrylic acid-co-*N*-*tert*-butylacrylamide) nanoparticles to find an optimal system for the molecular imprinting of proteins under mild conditions. Two redox activators, TEMED and SBS were tested in comparison with the widely used thermal activation of the initiator at 60 °C. While with thermal and SBS initiation the conversion rate of AAc was comparable to the other monomers, using TEMED the relative incorporation rate of AAc was extremely slow. This was attributed to the acid base reaction between AAc and TEMED. As a result, the other systems afforded almost homogeneous incorporation of AAc throughout the particle, but the TEMED activated reaction rendered AAc to accumulate almost exclusively in the outer shell of the nanoparticles. This, in turn, lead to a decreased binding of lysozyme.

Due to the inherent basic properties of TEMED, its application in the polymerization of multifunctional nanoparticles containing acidic monomers requires much attention and careful optimization. SBS, a similar redox activator of APS offers a viable alternative when the synthesis temperature should be kept low, because it affords nanoparticles with similar microstructure and protein binding properties as the thermally initiated polymerization.

#### Acknowledgement

The authors acknowledge the courtesy of Innovációs Laboratórium Ltd., (Miskolc, Hungary) for supporting the Field Emission Scanning Electron Microscope (SEM) Hitachi S-4800 equipped with Bruker AXS Energy-dispersive X-ray Spectrometer (EDS) system and thank Anna Sycheva for the SEM measurements. The research reported in this paper was supported by the BME Nanotechnology and Materials Science TKP2020 IE grant of NKFIH Hungary (BME IE-NAT TKP2020). Marwa A. Ahmed acknowledges the support of the Stipendium Hungaricum Scholarship.

## References

- [1] Pelton, R. H., Chibante, P. "Preparation of aqueous latices with *N*-isopropylacrylamide", *Colloids and Surfaces*, 20(3), pp. 247–256, 1986.  
[https://doi.org/10.1016/0166-6622\(86\)80274-8](https://doi.org/10.1016/0166-6622(86)80274-8)
- [2] Kawaguchi, H. "Thermoresponsive microhydrogels: Preparation, properties and applications", *Polymer International*, 63(6), pp. 925–932, 2014.  
<https://doi.org/10.1002/pi.4675>
- [3] Saunders, B. R., Laajam, N., Daly, E., Teow, S., Hu, X., Stepto, R. "Microgels: From responsive polymer colloids to bio-materials", *Advances in Colloid and Interface Science*, 147–148, pp. 251–262, 2009.  
<https://doi.org/10.1016/j.cis.2008.08.008>
- [4] Guan, Y., Zhang, Y. "PNIPAM microgels for biomedical applications: from dispersed particles to 3D assemblies", *Soft Matter*, 7(14), pp. 6375–6384, 2011.  
<https://doi.org/10.1039/C0SM01541E>
- [5] Lyon, L. A., Meng, Z., Singh, N., Sorrell, C. D., St. John, A. "Thermoresponsive microgel-based materials", *Chemical Society Reviews*, 38(4), pp. 865–874, 2009.  
<https://doi.org/10.1039/B715522K>
- [6] Welsch, N., Ballauff, M., Lu, Y. "Microgels as Nanoreactors: Applications in Catalysis", In: Pich, A., Richtering, W. (eds.) *Chemical Design of Responsive Microgels: Advances in Polymer Science*, Springer, Berlin, Heidelberg, Germany, 2011, pp. 129–163.  
[https://doi.org/10.1007/12\\_2010\\_71](https://doi.org/10.1007/12_2010_71)
- [7] Islam, M. R., Ahiabu, A., Li, X., Serpe, M. J. "Poly (*N*-isopropylacrylamide) Microgel-Based Optical Devices for Sensing and Biosensing", *Sensors*, 14(5), pp. 8984–8995, 2014.  
<https://doi.org/10.3390/s140508984>
- [8] Hoshino, Y., Shea, K. J. "The evolution of plastic antibodies", *Journal of Materials Chemistry*, 21(11), pp. 3517–3521, 2011.  
<https://doi.org/10.1039/c0jm03122d>
- [9] Debord, J. D., Lyon, L. A. "Synthesis and Characterization of pH-Responsive Copolymer Microgels with Tunable Volume Phase Transition Temperatures", *Langmuir*, 19(18), pp. 7662–7664, 2003.  
<https://doi.org/10.1021/la0342924>
- [10] Ogawa, K., Nakayama, A., Kokufuta, E. "Preparation and Characterization of Thermosensitive Polyampholyte Nanogels", *Langmuir*, 19(8), pp. 3178–3184, 2003.  
<https://doi.org/10.1021/la0267185>
- [11] Hoshino, Y., Urakami, T., Kodama, T., Koide, H., Oku, N., Okahata, Y., Shea, K. J. "Design of Synthetic Polymer Nanoparticles that Capture and Neutralize a Toxic Peptide", *Small*, 5(13), pp. 1562–1568, 2009.  
<https://doi.org/10.1002/smll.200900186>
- [12] Hoshino, Y., Haberaecker, W. W., Kodama, T., Zeng, Z., Okahata, Y., Shea, K. J. "Affinity Purification of Multifunctional Polymer Nanoparticles", *Journal of the American Chemical Society*, 132(39), pp. 13648–13650, 2010.  
<https://doi.org/10.1021/ja1058982>
- [13] Hoshino, Y., Koide, H., Furuya, K., Haberaecker, W. W., Lee, S. H., Kodama, T., Kanazawa, H., Oku, N., Shea, K. J. "The rational design of a synthetic polymer nanoparticle that neutralizes a toxic peptide in vivo", *Proceedings of the National Academy of Sciences of the United States of America*, 109(1), pp. 33–38, 2012.  
<https://doi.org/10.1073/pnas.1112828109>
- [14] Hoshino, Y., Koide, H., Urakami, T., Kanazawa, H., Kodama, T., Oku, N., Shea, K. J. "Recognition, Neutralization, and Clearance of Target Peptides in the Bloodstream of Living Mice by Molecularly Imprinted Polymer Nanoparticles: A Plastic Antibody", *Journal of the American Chemical Society*, 132(19), pp. 6644–6645, 2010.  
<https://doi.org/10.1021/ja102148f>
- [15] Yoshimatsu, K., Lesel, B. K., Yonamine, Y., Beierle, J. M., Hoshino, Y., Shea, K. J. "Temperature-Responsive "Catch and Release" of Proteins by using Multifunctional Polymer-Based Nanoparticles", *Angewandte Chemie - International Edition*, 51(10), pp. 2405–2408, 2012.  
<https://doi.org/10.1002/anie.201107797>
- [16] Beierle, J. M., Yoshimatsu, K., Chou, B., Mathews, M. A. A., Lesel, B. K., Shea, K. J. "Polymer Nanoparticle Hydrogels with Autonomous Affinity Switching for the Protection of Proteins from Thermal Stress", *Angewandte Chemie - International Edition*, 53(35), pp. 9275–9279, 2014.  
<https://doi.org/10.1002/anie.201404881>
- [17] Lee, S. H., Hoshino, Y., Randall, A., Zeng, Z., Baldi, P., Doong, R., Shea, K. J. "Engineered Synthetic Polymer Nanoparticles as IgG Affinity Ligands", *Journal of the American Chemical Society*, 134(38), pp. 15765–15772, 2012.  
<https://doi.org/10.1021/ja303612d>
- [18] Koide, H., Yoshimatsu, K., Hoshino, Y., Lee, S. H., Okajima, A., Ariizumi, S., Narita, Y., Yonamine, Y., Weisman, A. C., Nishimura, Y., Oku, N., Miura, Y., Shea, K. J. "A polymer nanoparticle with engineered affinity for a vascular endothelial growth factor (VEGF<sub>165</sub>)", *Nature Chemistry*, 9(7), pp. 715–722, 2017.  
<https://doi.org/10.1038/nchem.2749>
- [19] Wulff, G. "Molecular Imprinting in Cross-Linked Materials with the Aid of Molecular Templates— A Way towards Artificial Antibodies", *Angewandte Chemie International Edition*, 34(17), pp. 1812–1832, 1995.  
<https://doi.org/10.1002/anie.199518121>
- [20] Vlatakis, G., Andersson, L. I., Müller, R., Mosbach, K. "Drug assay using antibody mimics made by molecular imprinting", *Nature*, 361(6413), pp. 645–647, 1993.  
<https://doi.org/10.1038/361645a0>
- [21] Ye, L. "Molecular Imprinting: Principles and Applications of Micro- and Nanostructure Polymers", CRC press, Boca Raton, FL, USA, 2013.
- [22] Hoshino, Y., Kodama, T., Okahata, Y., Shea, K. J. "Peptide Imprinted Polymer Nanoparticles: A Plastic Antibody", *Journal of the American Chemical Society*, 130(46), pp. 15242–15243, 2008.  
<https://doi.org/10.1021/ja8062875>

- [23] Poma, A., Guerreiro, A., Whitcombe, M. J., Piletska, E. V., Turner, A. P. F., Piletsky, S. A. "Solid-Phase Synthesis of Molecularly Imprinted Polymer Nanoparticles with a Reusable Template - "Plastic Antibodies"", *Advanced Functional Materials*, 23(22), pp. 2821–2827, 2013.  
<https://doi.org/10.1002/adfm.201202397>
- [24] Guerreiro, A., Poma, A., Karim, K., Moczko, E., Takarada, J., Perez de Vargas-Sansalvador, I., Turner, N., Piletska, E., Schimdt de Magalhães, C. S., Glazova, N., Serkova, A., Omelianova, A., Piletsky, S. "Influence of Surface-Imprinted Nanoparticles on Trypsin Activity", *Advanced Healthcare Materials*, 3(9), pp. 1426–1429, 2014.  
<https://doi.org/10.1002/adhm.201300634>
- [25] Cecchini, A., Raffa, V., Canfarotta, F., Signore, G., Piletsky, S., MacDonald, M. P., Cuschieri, A. "In Vivo Recognition of Human Vascular Endothelial Growth Factor by Molecularly Imprinted Polymers", *Nano Letters*, 17(4), pp. 2307–2312, 2017.  
<https://doi.org/10.1021/acs.nanolett.6b05052>
- [26] Moczko, E., Guerreiro, A., Cáceres, C., Piletska, E., Sellergren, B., Piletsky, S. A. "Epitope approach in molecular imprinting of antibodies", *Journal of Chromatography B*, 1124, pp. 1–6, 2019.  
<https://doi.org/10.1016/j.jchromb.2019.05.024>
- [27] Xu, J., Merlier, F., Avalle, B., Vieillard, V., Debré, P., Haupt, K., Tse Sum Bui, B. "Molecularly Imprinted Polymer Nanoparticles as Potential Synthetic Antibodies for Immunoprotection against HIV", *ACS Applied Materials & Interfaces*, 11(10), pp. 9824–9831, 2019.  
<https://doi.org/10.1021/acsami.8b22732>
- [28] Hu, X., Tong, Z., Lyon, L. A. "Control of Poly(*N*-isopropylacrylamide) Microgel Network Structure by Precipitation Polymerization near the Lower Critical Solution Temperature", *Langmuir*, 27(7), pp. 4142–4148, 2011.  
<https://doi.org/10.1021/la200114s>
- [29] Rodriguez, F., Givay, R. D. "Polymerization of acrylamide with persulfate-metabisulfite initiator", *Journal of Polymer Science*, 55(162), pp. 713–719, 1961.  
<https://doi.org/10.1002/pol.1961.1205516224>
- [30] Orakdogan, N., Okay, O. "Influence of the initiator system on the spatial inhomogeneity in acrylamide-based hydrogels", *Journal of Applied Polymer Science*, 103(5), pp. 3228–3237, 2007.  
<https://doi.org/10.1002/app.24977>
- [31] Kabiri, K., Zohuriaan-Mehr, M. J., Bouhendi, H., Jamshidi, A., Ahmad-Khanbeigi, F. "Residual monomer in superabsorbent polymers: Effects of the initiating system", *Journal of Applied Polymer Science*, 114(4), pp. 2533–2540, 2009.  
<https://doi.org/10.1002/app.30785>
- [32] Gasztych, M., Kotowska, A., Musial, W. "Application of Polymerization Activator in the Course of Synthesis of *N*-Isopropylacrylamide Derivatives for Thermally Triggered Release of Naproxen Sodium", *Materials*, 11(2), Article Number: 261, 2018.  
<https://doi.org/10.3390/ma11020261>
- [33] Bao, L., Zha, L. "Preparation of Poly(*N*-isopropylacrylamide) Microgels using Different Initiators Under Various pH Values", *Journal of Macromolecular Science, Part A: Pure and Applied Chemistry*, 43(11), pp. 1765–1771, 2006.  
<https://doi.org/10.1080/10601320600939528>
- [34] Wang, Z., Xue, M., Zhang, H., Meng, Z., Shea, K. J., Qiu, L., Ji, T., Xie, T. "Self-assembly of a nano hydrogel colloidal array for the sensing of humidity", *RSC Advances*, 8(18), pp. 9963–9969, 2018.  
<https://doi.org/10.1039/C7RA12661A>
- [35] Yoshimatsu, K., Yamazaki, T., Hoshino, Y., Rose, P. E., Epstein, L. F., Miranda, L. P., Tagari, P., Beierle, J. M., Yonamine, Y., Shea, K. J. "Epitope Discovery for a Synthetic Polymer Nanoparticle: A New Strategy for Developing a Peptide Tag", *Journal of the American Chemical Society*, 136(4), pp. 1194–1197, 2014.  
<https://doi.org/10.1021/ja410817p>
- [36] Korposh, S., Chianella, I., Guerreiro, A., Caygill, S., Piletsky, S., James, S. W., Tatam, R. P. "Selective vancomycin detection using optical fibre long period gratings functionalised with molecularly imprinted polymer nanoparticles", *Analyst*, 139(9), pp. 2229–2236, 2014.  
<https://doi.org/10.1039/c3an02126b>
- [37] Shugar, D. "The measurement of lysozyme activity and the ultra-violet inactivation of lysozyme", *Biochimica et Biophysica Acta*, 8, pp. 302–309, 1952.  
[https://doi.org/10.1016/0006-3002\(52\)90045-0](https://doi.org/10.1016/0006-3002(52)90045-0)
- [38] Odian, G. "Principles of Polymerization", John Wiley & Sons, Inc., Hoboken, NJ, USA, 2004.  
<https://doi.org/10.1002/047147875X>
- [39] Virtanen, O. L. J., Kather, M., Meyer-Kirschner, J., Melle, A., Radulescu, A., Viell, J., Mitsos, A., Pich, A., Richtering, W. "Direct Monitoring of Microgel Formation During Precipitation Polymerization of *N*-Isopropylacrylamide Using in Situ SANS", *ACS Omega*, 4(2), pp. 3690–3699, 2019.  
<https://doi.org/10.1021/acsomega.8b03461>
- [40] Wu, X., Pelton, R. H., Hamielec, A. E., Woods, D. R., McPhee, W. "The kinetics of poly(*N*-isopropylacrylamide) microgel latex formation", *Colloid and Polymer Science*, 272(4), pp. 467–477, 1994.  
<https://doi.org/10.1007/BF00659460>
- [41] Varga, I., Gilányi, T., Mészáros, R., Filipcsei, G., Zrínyi, M. "Effect of Cross-Link Density on the Internal Structure of Poly(*N*-isopropylacrylamide) Microgels", *The Journal of Physical Chemistry B*, 105(38), pp. 9071–9076, 2001.  
<https://doi.org/10.1021/jp004600w>
- [42] Hoare, T., McLean, D. "Kinetic Prediction of Functional Group Distributions in Thermosensitive Microgels", *The Journal of Physical Chemistry B*, 110(41), pp. 20327–20336, 2006.  
<https://doi.org/10.1021/jp0643451>
- [43] Lacík, I., Beuermann, S., Buback, M. "PLP-SEC Study into the Free-Radical Propagation Rate Coefficients of Partially and Fully Ionized Acrylic Acid in Aqueous Solution", *Macromolecular Chemistry and Physics*, 205(8), pp. 1080–1087, 2004.  
<https://doi.org/10.1002/macp.200300251>
- [44] Cutié, S. S., Smith, P. B., Henton, D. E., Staples, T. L., Powell, C. "Acrylic acid polymerization kinetics", *Polymer Science Part B: Polymer Physics*, 35(13), pp. 2029–2047, 1997.  
[https://doi.org/10.1002/\(SICI\)1099-0488\(19970930\)35:13<2029::AID-POLB4>3.3.CO;2-K](https://doi.org/10.1002/(SICI)1099-0488(19970930)35:13<2029::AID-POLB4>3.3.CO;2-K)
- [45] Kabanov, V. A., Topchiev, D. A., Karaputadze, T. M. "Some features of radical polymerization of acrylic and methacrylic acid salts in aqueous solutions", *Journal of Polymer Science: Polymer Symposia*, 42(1), pp. 173–183, 1973.  
<https://doi.org/10.1002/polc.5070420120>

- [46] Caglio, S., Righetti, P. G. "On the pH dependence of polymerization efficiency, as investigated by capillary zone electrophoresis", *Electrophoresis*, 14(1), pp. 554–558, 1993.  
<https://doi.org/10.1002/elps.1150140184>
- [47] Feng, X. D., Guo, X. Q., Qiu, K. Y. "Study of the initiation mechanism of the vinyl polymerization with the system persulfate/*N,N,N',N'*-tetramethylethylenediamine", *Die Makromolekulare Chemie*, 189(1), pp. 77–83, 1988.  
<https://doi.org/10.1002/macp.1988.021890108>